LENGTH AND BURSTING OF SEPARATION BUBBLES: A PHYSICAL

INTERPRETATION[*]

John M. Russell
Department of Aeronautics and Astronautics
Massachusetts Institute of Technology

SUMMARY

A physical interpretation of the observed form of the pressure distribution beneath a two-dimensional "short" separation bubble (which modifies the external inviscid pressure distribution only locally) is given in terms of boundary layer concepts (i.e., constancy of static pressure across the layer as long as the layer is "thin"). At the mean separation and reattachment points (which lie on the same mean streamline), the local static pressure equals the local stagnation pressure, since the velocity is zero at these points. The boundary layer hypothesis then implies that reattachment can only occur at a point $x - x_s$ downstream of the separation point x_s if the jump in external inviscid static pressure $\frac{\rho}{2}\left[U^2(x) - U^2(x_s)\right]$ is less than or equal to the rise in stagnation pressure $H(x) - H(x_s)$ along the separation streamline after separation. A simple method for estimating the growth of $H(x)$ along a mean streamline entrained into the underside of a growing shear layer through the transition region is discussed, and predictions of bubble bursting conditions and a lower bound on the bubble length are compared with experiment.

INTRODUCTION

Since the early work of Melvill Jones (ref. 1), it has been known experimentally that a laminar boundary layer on an airfoil, after entry into a region of adverse pressure gradient strong enough to cause laminar separation, will separate in the laminar state, sometimes achieve transition to turbulent flow in the separated shear layer, and (if the adverse pressure gradient is not too severe) reattach to the surface to form a closed recirculating flow eddy known as a separation bubble. In a typical case (fig. 1), the turbulent boundary layer downstream of the reattachment point R either does not separate at all over the remaining portion of the upper surface or separates only a short distance upstream of the trailing edge. In such a flow, the form of the external static pressure distribution outside of the region of separation is approximated

reasonably well by the potential flow pressure distribution, though the magnitude of the actual pressure is somewhat smaller. It follows that the lift of an airfoil with this type of bubble separation is approximately equal to the value predicted by inviscid theory. Following Tani (ref. 2), we will refer to this flow phenomenon as a separation bubble of the "short" type, to distinguish it from another type of closed recirculating flow in which the entire pressure distribution differs radically from the potential flow form. The latter is referred to as a "long" bubble.

Separation bubbles are of great importance in engineering because of the role they play in the phenomenon of airfoil stalling, which may sometimes be identified with a transition of the flow from a short type of bubble separation to the long type. This abrupt transition, known as "bursting" of the short bubble, is in some cases responsible for producing the well-known "critical" Reynolds number region in the plot of drag coefficient versus Reynolds number for circular cylinders and spheres (ref. 2) and for moderately thick airfoils at Reynolds numbers lower than about 10^5 (refs. 3 and 4).

Reference 2 contains a thorough background discussion of the phenomenon of separation bubbles and a review of the experimental work prior to 1964. Reference 5 reviews most of the more recent experimental work up to 1976. The reader is referred to these sources for general information about the subjects treated in this paper.

In recent years, there have been several attempts to develop semi-empirical calculation methods for predicting the length and bursting conditions for separation bubbles of the short type. These range in sophistication from solution of the full time-dependent two-dimensional Navier-Stokes equations (with modeling of the turbulence), as in reference 7, to simpler modifications of existing boundary layer calculation methods incorporating iterative methods to account for viscous-inviscid interaction between the external stream and the flow within the bubble (refs. 6 and 8). All of these methods use experimental data on separation bubbles to fix the values of certain numerical coefficients appearing in the theory. In each case, the shape of the separation streamline and the external pressure distribution between separation and reattachment are unknowns in the problem and are not determined until the calculation is finished. Since the distributions of these quantities play a crucial role in determining the length and bursting of the bubble, there is some difficulty in using the numerical prediction methods (or the theories on which they are based) to deepen one's understanding of the fundamental physical processes controlling the flow.

The objectives of the present study are to explain why reattachment occurs at all, to explain why the observed pressure distribution has its characteristic form, and to develop a shortcut method for calculating the length of a short separation bubble, if one exists, or to determine the conditions under which a short bubble cannot exist.

PHYSICAL MODEL

The Cause of Reattachment

The principal cause of turbulent reattachment following laminar separation has been discussed by Cebici and Bradshaw (ref. 9). Consider the separation of a laminar boundary layer from a smooth surface as shown in figure 2. The edge of the shear layer has been drawn to show the spreading of the shear layer in the downstream direction due initially to laminar and later to turbulent mixing of momentum. This spreading results in a greater mass flux across the segment BB' in figure 2 than across the segment AA'. In two-dimensional flow, mass conservation requires that there be a net inflow across the segment AB. This entrainment of fluid into the underside of a growing shear layer will be greatly increased by the transition from laminar to turbulent flow. If this entrainment rate is greater than any reversed flow coming from far downstream, then the shear layer simply sucks itself back onto the surface from which it separated (ref. 9, p. 366) to form the short separation bubble shown in figure 3, in which the entrainment flow is supplied by the splitting of the shear layer at reattachment.

The Form of the Pressure Distribution

In trying to identify the most important factors controlling the dynamics of separation bubbles, it is useful to see how many of the qualitative features of the flow can be accounted for adequately by simple boundary layer concepts. If, for example, simple boundary layer theory is found to account adequately for the observed length and pressure distribution of a bubble, then one can infer that the direct effects of streamline curvature and nonzero pressure gradients in the cross-stream direction (which are neglected in boundary layer theory) are indeed unimportant, at least in determining the gross qualitative features of the flow. This process of testing hypotheses that certain terms in the equations of motion are negligible will serve to increase our understanding of what a separation bubble is if it allows us to identify the few important from among the many unimportant effects operating at once in the flow.

In this spirit, we attempt to explain the characteristic pressure distribution beneath a short separation bubble (cf. fig. 1) by supposing that the assumptions of classical boundary layer theory hold. In particular, the static pressure across the separation bubble in figure 3 is assumed to be constant, and the velocity component in the direction normal to the wall is assumed to be an order of magnitude smaller than the component parallel to the wall. With these assumptions, the pressure distribution along the wall between points S and R in figure 3 can be inferred. The pressure gradient between points S and K must be small since the velocities and shear stresses in the slowly moving interior of the bubble are driven only by entrainment and are, therefore, small. In the region downstream of the point K, the streamwise velocity along each closed recirculating flow streamline will be zero at the downstream extremity of that streamline. Since the vertical velocity at such a downstream extremity is small, the static pressure is very nearly equal to the local stagnation pressure at that point. It follows that the distribution of pressure along the line connecting all such downstream extremities of streamlines (represented as the

dotted line in fig. 3) will approximately equal the distribution of stagnation pressure between the lower edge of the shear layer (at point K) and the separation streamline (at point R). This difference in stagnation pressures may be substantial because the velocity on the separation streamline (which lies close to the center of the shear layer at the streamwise station K) will typically be much larger than the velocity on the lower edge of the shear layer at any given streamwise station.

In general, we expect the pressure distribution beneath the separation bubble in figure 3 to be as shown in figure 4, which is in good qualitative agreement with the examples of short separation bubbles in reference 2. The rather sharp corner in the pressure distribution in figure 4 is interpreted here as the point where the lower edge of the shear layer impinges on the wall. According to our model, this point also coincides with the center of the innermost closed streamline in figure 3. Note that the point K is not identified with the transition from laminar to turbulent flow (which we assume takes place somewhere upstream of the point K).

It has been assumed in all experimental studies on separation bubbles known to the author that the sharp corner in the pressure distribution coincides with the transition point. Gault (ref. 10) proposes this as a means of experimentally determining transition, while Van Ingen (ref. 11) uses the same assumption to fix the numerical values of the adjustable constants in a form of his "e to the ninth" method for transition prediction, developed especially for use in separation bubbles. In view of the fact that transition from laminar to turbulent flow occurs quite readily in a free shear layer in zero pressure gradient without modifying the static pressure, one is at a loss to see why transition as such should have any effect on the pressure distribution at all, much less account for the abrupt, nearly discontinuous pressure rise that occurs at the rear of a short separation bubble. The rather arbitrary and ad hoc character of the conventional interpretation of the pressure distribution renders it less favorable from a fundamental viewpoint than the interpretation in terms of stagnation pressures given above.

Length and Bursting of Short Bubbles

We have included among the defining features of short separation bubbles the condition that the bubble modify only locally the static pressure distribution about the body on which the bubble occurs; that is, the pressure distribution everywhere ahead of and behind the bubble is approximately equal to the value predicted by potential theory. In particular, the pressures at the separation and reattachment points (which are the inner limits of the portion of the pressure distribution lying outside the bubble) must both be points lying very near the inviscid pressure distribution curve. These endpoint conditions, together with our model of the pressure distribution within the bubble in terms of stagnation pressures on the recirculating flow streamlines, provide a clue as to what determines the length of a short separation bubble, when it is possible for one to exist, and why it is sometimes impossible for a short bubble to exist.

Now the difference in static pressure between the points S and R in figure 3 equals the net rise in stagnation pressure along the separation streamline, since the velocity is zero at both endpoints. It follows that if a plot of the rise in stagnation pressure along the separation streamline downstream of separation is drawn on the same graph as the rise in inviscid static pressure downstream of the same point, then an estimate of the bubble length is the streamwise distance from separation to the first point where the curves cross.

One difficulty with such a graphical procedure for the calculation of the bubble length is that the curves may cross at more than one point, giving a choice of several possible bubble lengths rather than a single one. Another difficulty is that the stagnation pressure along the whole length of the separation streamline is not known under general conditions. It can, however, be estimated by assuming that the growth of the shear layer downstream of separation is nearly equal to that of a free shear layer in zero pressure gradient, for which the mean velocity and, hence, stagnation pressure and stream function profiles are known from experiments on transition in a laminar mixing layer (ref. 12).

A calculation based on similar physical concepts was made by Tani (ref. 2) to estimate the maximum attainable value of the coefficient of pressure recovery within a bubble σ defined by the relation

$$\sigma = \frac{p_R - p_S}{\frac{\rho}{2} U_S^2} \tag{1}$$

Owen and Klanfer (ref. 13) had proposed the value $\sigma_{max} = 0.35$ from experimental evidence. By noting that the velocity along any streamline entrained into the low velocity side of a growing shear layer cannot exceed the velocity on the dividing streamline $(u/U)_{D.S.} = 0.5873 \ldots$, Tani argued that a lower bound on the nondimensional stagnation pressure rise existed and was given by

$$\left(\frac{\Delta H}{\frac{\rho}{2} U_S^2} \right)_{max} = \left[(u/U)_{D.S.} \right]^2 = 0.3449 \ldots \tag{2}$$

which is in excellent agreement with the figure 0.35 given by Owen and Klanfer. Tani did not suggest the extension of the stagnation pressure idea to the calculation of the bubble length, however.

The method of estimating the reattachment position as the streamwise coordinate of the point of intersection of the curves of inviscid pressure rise and stagnation pressure rise on the separation streamline after separation provides a necessary condition for the existence of a short bubble, namely, that the two curves indeed intersect. A possible condition for the impossibility of a short separation bubble (i.e., a "bursting" condition) might then be that the inviscid

pressure gradient downstream of separation be so steep that the two curves never intersect. The borderline case in which a short bubble is just barely possible, but would become impossible with an infinitesimal increase in the inviscid pressure gradient, is when the two curves are tangent to each other at a single point. Later in this paper we will use this tangency condition to derive a close approximation to Gaster's "bursting line" (ref. 14), which has been found by several experimentalists (see ref. 5) to be a reliable empirical formula for predicting the boundary between the short and long type of bubble separations.

DEVELOPMENT OF THE SHEAR LAYER

For reasons indicated in the last section, it is desirable to have an explicit formula for the development of the stagnation pressure $H(s)$ along the separation streamline in a short bubble.

For simplicity, we will assume that the actual distribution of stagnation pressure along the separation streamline can be approximated by the stagnation pressure distribution along a particular streamline entrained into the underside of a self-similar shear layer in zero pressure gradient, for which the velocity profile has been calculated from the Blasius equation in the laminar case (ref. 15), and has been measured experimentally in the transitional and fully turbulent cases (refs. 12 and 16, respectively). It has been found experimentally (cf. ref. 12, fig. 12) that the functional form of the mean velocity profile is experimentally indistinguishable for these three cases, the effect of transition being a large and abrupt increase of the rate of spreading of the shear layer measured by, say, the growth of the momentum thickness $\theta(s)$.

Before treating the problems of the location of the transition region, the growth of the resulting turbulent layer, and the determination of the value of the stream function (relative to the reference streamline in a self-similar shear layer) appropriate for representing the separation streamline in a separation bubble, it is necessary to recall certain properties of self-similar shear layers, and, in particular, to obtain explicit approximate formulas for the velocity and stream function profiles.

The Laminar Shear Layer

The nomenclature for self-similar shear layers is as shown in figure 5, which illustrates the flow downstream of a hypothetical splitter plate, the upper surface of which moves with the velocity U_1 (precluding the formation of a boundary layer there), while the lower surface is stationary. The fluid above the plate ($x < 0$, $y > 0$) moves with the uniform velocity U_1 while the fluid below the plate ($x < 0$, $y < 0$) is at rest. The effect of these boundary conditions is the elimination of any length scale other than the streamwise coordinate x, so that self-similarity in laminar flow is to be expected.

The steady two-dimensional Prandtl boundary layer equations for zero pressure gradient,

$$u \frac{\partial u}{\partial x} + v \frac{\partial u}{\partial y} = \frac{\partial^2 u}{\partial y^2} \tag{3}$$

$$\frac{\partial u}{\partial x} + \frac{\partial v}{\partial y} = 0 \tag{4}$$

thus reduce to the Blasius equation,

$$2 f'''(\eta) + ff''(\eta) = 0 \tag{5}$$

in the usual way (e.g., ref. 17, p. 126), where

$$\eta = y \left(\frac{U_1}{\nu x}\right)^{1/2} = \frac{y}{\ell(x)} \tag{6}$$

$$f(\eta) = \frac{\psi(x,y)}{(\nu U_1 x)^{1/2}} = \frac{\psi(x,y)}{U_1 \ell(x)} \tag{7}$$

$$u = \frac{\partial \psi}{\partial y} = U_1 f'(\eta) \qquad v = -\frac{\partial \psi}{\partial x} = \frac{1}{2}\left(\frac{U_1 \nu}{x}\right)\left[\eta f'(\eta) - f(\eta)\right] \tag{8}$$

The boundary conditions appropriate for a free shear layer are

$$u \to U_1 \Rightarrow f' \to 1 \quad \text{as} \quad \eta \to +\infty \tag{9}$$

$$u \to 0 \Rightarrow f' \to 0 \quad \text{as} \quad \eta \to -\infty \tag{10}$$

$$\psi = f = v = 0 \quad \text{when} \quad \eta = 0 \tag{11}$$

The exact solution of equation (5) satisfying the boundary conditions (9), (10), and (11) has been tabulated by Lock (ref. 15) to four significant figures. The tabulated solution provides a useful check on the accuracy of approximate representations of the velocity profile in terms of elementary functions.

183

Approximation of the Velocity Profile

For the present purpose, it is sufficient to obtain an approximate solution to equation (5) in terms of elementary functions whose forms are chosen to reproduce as many of the properties of the exact solution as is convenient. For example, the condition $f(0) = 0$ implies that $f'''(0) = 0$ (from equation (5)), so that the velocity f' has an inflection point at the origin, or, equivalently, the shear stress is maximum there. In addition, the conditions $f(\eta) \approx \eta$ as $\eta \to +\infty$ and $f(\eta) \approx$ Constant as $\eta \to -\infty$ imply that f' behaves like a complementary error function for large positive η and like a simple exponential for large negative η. These conditions, together with the requirement that the velocity profile be a smooth monotonic function of η, suggest the approximate forms

$$\eta > 0: \quad f'(\eta) = 1 - \left[1 - f'(0)\right] \frac{2}{\sqrt{\pi}} \int_{a\eta/2}^{\infty} e^{-x^2}\, dx \tag{12}$$

$$\eta < 0: \quad f'(\eta) = f'(0) \frac{3}{2} \operatorname{sech}^2 \left[b\eta + \tanh^{-1}\left(\frac{1}{\sqrt{3}}\right)\right] \tag{13}$$

each of which has an inflection point at $\eta = 0$ and the correct asymptotic behavior as $|\eta| \to \infty$. Equations (12) and (13) are constructed so that the velocity $f'(\eta)$ is continuous at the juncture $\eta = 0$. The requirement that the slope of the velocity be continuous at $\eta = 0$ provides one equation relating the constants a and b:

$$-\left[1 - f'(0)\right] a\left(\frac{-1}{\sqrt{\pi}}\right) = f'(0)\left(\frac{-2}{\sqrt{3}}\right)b \tag{14}$$

Equation (14) provides an expression for the ratio a/b in terms of $f'(0)$, where either a or b remains free to be determined by a suitable normalization.

The only important unknown that remains is now $f'(0)$, which we will determine by a momentum integral method. Integrating equation (5) from $-\infty$ to 0, we obtain

$$2\, f''\Big]_{-\infty}^{0} + ff'\Big]_{-\infty}^{0} - \int_{-\infty}^{0} (f')^2\, d\eta = 0$$

while the integral from 0 to ∞ gives

$$2 \left. f'' \right]_0^\infty + f(f' - 1) \left. \right]_0^\infty - \int_0^\infty f'(-1 + f') \ d\eta = 0$$

Applying the boundary conditions for a shear layer, these equations become

$$2 \ f''(0) = \int_{-\infty}^0 (f')^2 \ d\eta = \int_0^\infty f'(1 - f') \ d\eta \tag{15}$$

which are forms of the Von Kármán momentum integral equation (e.g., ref. 17, p. 146) for each half of the flow, and which have direct counterparts when the flow is turbulent (e.g., ref. 18, p. 227).

If equations (12), (13), and (14) are substituted into equation (15), then a cubic equation for the quantity $1 - f'(0)$ is obtained (see appendix), the relevant solution of which gives $f'(0) = 0.58923$, which agrees well with the tabulated value $f'(0) = 0.5873$ in reference 15.

For our normalization condition (needed to determine either a or b from equation (14)), we note that equation (15) implies

$$\frac{\theta}{\ell} \equiv \theta^* = \int_{-\infty}^0 f'(1 - f') \ d\eta + \int_0^\infty f'(1 - f') \ d\eta$$

$$= \left. f \right]_{-\infty}^0 - f''(0) + f''(0) = -f(-\infty) \tag{16}$$

which according to reference 16, has the numerical value $-f(-\infty) = 1.2386$.

It follows from equations (12), (13), (14), and (16) (see appendix) that $a = 0.88544$ and $b = -0.30160$, which completely determines all of the constants in our approximate velocity profile. For $\eta < 0$ (which is the region of interest in the separation bubble problem), the approximate velocity profile given by equation (13) is uniformly accurate to within 1 percent of the tabulated values in reference 16.

Development of the Momentum Thickness

The nondimensional velocity profile $f'(\eta)$, together with the definition of the transverse length scale $\ell(x)$ in equation (6) and the free stream velocity U_1 completely determine the flow in a laminar shear layer. It is convenient to express $\ell(x)$ in terms of information available at a station $x = x_1$, rather than in terms of the distance x downstream of the splitter plate in figure 5. From equation (6),

$$\ell(x) = \left(\frac{\nu x}{U_1}\right)^{1/2} = \left[\frac{\nu(x - x_1)}{U_1} + \ell(x_1)^2\right]^{1/2}$$

$$= \ell_1\left[\frac{1}{\left(\frac{U_1\ell_1}{\nu}\right)} \cdot \frac{x - x_1}{\ell_1} + 1\right]^{1/2}$$

where ℓ_1 is defined to be $\ell(x_1)$. Rewriting in terms of the momentum thickness $\theta(x_1)$ and using the fact that $\theta(x)/\ell(x) = \theta^* = 1.2386$, we have

$$\frac{\theta(x)}{\theta(x_1)} = \left\{\frac{(\theta/\ell)^2}{\left[\frac{U_1 \theta(x_1)}{\nu}\right]} \frac{x - x_1}{\theta(x_1)} + 1\right\}^{1/2} \qquad \text{(Laminar flow)} \qquad (17)$$

As mentioned before, we will assume that the functional form of the mean velocity profile in a self-similar turbulent shear layer is the same as in laminar flow. Thus, we continue to use equations (12) and (13) for the velocity profile, though the definition of the transverse length scale $\ell(x)$ (which equals $(\nu x/U_1)^{1/2}$ in laminar flow) must be altered. Since the equation $\theta = \theta^* \ell(x)$ holds in general, this may serve as the definition of $\ell(x)$ in turbulent flow, provided that an adequate empirical formula for the development of $\theta(x)$ can be found.

From the data of Sato (ref. 12), such a formula is not hard to develop. We may take, for example, in the transitional and fully turbulent regions of the flow

$$\frac{\theta(x)}{\theta_s} = \left[\frac{\theta(x)}{\theta_s}\right]_{\text{lam}} + \left[\frac{\theta}{\theta_s}\right]_{\text{extra}} \qquad (18)$$

where, for $(x - x_s)/\theta_s \gtreqless N_t$,

$$\left[\frac{\theta}{\theta_s}\right]_{\text{extra}} = 0.046\left[\left(\frac{x - x_s}{\theta_s} - N_t\right) + \frac{\lambda_1}{\theta_s} \tanh\left(\frac{\frac{x - x_s}{\theta_s} - N_t}{\frac{\lambda_2}{\theta_s}}\right)\right] \qquad (19)$$

and where $\left[\theta(x)/\theta_s\right]_{lam}$ is given by equation (17) with $x_1 = x_s$. A plot of equation (19) with the numerical values $\lambda_1/\theta_s = 34$, $\lambda_2/\theta_s = 135$, and $N_t = 56$ is shown in figure 6. Also shown are the measured values of $\theta(x)/\theta_s - \left[\theta(x)/\theta_s\right]_{lam}$ for three different flows in reference 12. The agreement is seen to be quite reasonable.

The condition $(s - x_s)/\theta_s = N_t$ represented a transition criterion and appears to hold quite generally for two-dimensional laminar separated flows of the type under discussion. For example, figure 12 of Freymuth (ref. 19), which shows the growth of the streamwise fluctuation velocity component $|u'|_{max}$ in a free shear layer downstream of separation for a variety of separation Reynolds numbers, indicates that the range of $(x - x_s)\theta_s$ in which the disturbances grow exponentially is almost completely independent of Reynolds number for $61 \leqq R_{\theta_s} \leqq 334$. This range was found to be $0 \leqq (x - x_s)/\theta_s \leqq 60$. Strong non-linearity (indicating the onset of transition) appears for $(x - x_s)/\theta_s \geqq 60$, which agrees well with the value $N_t = 56$ used here. A similar independence of the onset of transition with Reynolds number can be found in separation bubbles. For example, Gaster's results (ref. 14, fig. 11) of intermittency measurements in seven short separation bubbles in the range $136 \leqq R_{\theta_s} \leqq 394$ show that the onset of transition occurs for $50 \leqq (x - x_s)/\theta_s \leqq 80$ for all but one of the bubbles. Unlike the case of fully attached flow, it therefore appears that transition in fully separated flow is relatively easy to predict in terms of the critical value of a single parameter, at least in the case of nominally two-dimensional incompressible flow in the Reynolds number range under discussion under conditions of small background turbulence and acoustic noise.

VELOCITY DISTRIBUTION ALONG A STREAMLINE

The stream function ψ can be obtained from our approximate velocity profile (13) by integration. Applying the boundary condition $\psi = 0$ on $\eta = 0$, we have, from equations (7) and (13),

$$\psi = U_1 \, \ell(x) \, f(\eta) = \frac{U_1 \, \ell(x)}{b} \, \frac{3}{2} \, f'(0) \left\{ \tanh\left[b\eta + \tanh^{-1}\left(\frac{1}{\sqrt{3}}\right) \right] - \frac{1}{\sqrt{3}} \right\} \qquad (20)$$

Now the value of the stream function at $\eta = -\infty$, which represents the mass flow across the entire lower half of the shear layer in figure 5, is a function of x and may be used to define the (constant) stream function along the streamline that just enters the underside of the shear layer at any station x. In our model of the separation bubble, we will suppose that the separation point $x = x_s$ corresponds to the point where the separation streamline enters the underside of the separated shear layer in a bubble in just this way. That is, we will take

$$\psi_s = U_s \, \ell(x_s) \, f(-\infty) = -U_s \theta_s \qquad (21)$$

187

as the value of the stream function (relative to the shear layer) that repre-
sents the separation streamline in a bubble.

The distribution of velocity along the streamline $\psi = \psi_S$ can now be found
easily. From equations (20) and (21) (with $U_1 = U_S$), we have

$$\tanh\left[b\eta + \tanh^{-1}\left(\frac{1}{\sqrt{3}}\right)\right] = -\frac{\theta_S}{\theta}\frac{2b}{3\,f'(0)}\left(\frac{\theta}{\ell}\right) + \frac{1}{\sqrt{3}} \tag{22}$$

It follows from equation (13) and the identity $\text{sech}^2(x) = 1 - \tanh^2(x)$ that

$$\left(\frac{u}{U}\right)^2_{\psi=\psi_S} = \left[f'(\eta)\right]^2_{\psi=\psi_S} = \left(f'(0)\frac{3}{2}\left\{1 - \left[\frac{-2b\theta^*}{3\,f'(0)}\frac{\theta_S}{\theta} + \frac{1}{\sqrt{3}}\right]^2\right\}\right)^2 \tag{23}$$

Figure 7 is a plot of equation (23) for various separation Reynolds numbers.
Equations (17) through (19) have been used to evaluate the quantity θ/θ_S.

STAGNATION PRESSURE ALONG $\psi = \psi_S$

Equation (23), which was calculated from the known behavior of a free shear
layer in zero pressure gradient, provides a measure of the stagnation pressure
distribution along the streamline $\psi = \psi_S$, since in zero pressure gradient, the
stagnation pressure $H(x,\psi)$, defined by

$$H(x,\psi) = p + \frac{\rho}{2}u^2 \tag{24}$$

is simply equal to the dynamic pressure $(\rho/2)u^2$.

We recall that in a general shear flow, the stagnation pressure varies
along a mean streamline according to the approximate equation

$$\frac{\partial H}{\partial s} = \frac{\partial \tau}{\partial n} \tag{25}$$

where τ is the combined viscous and turbulent shear stress

$$\tau = \mu\frac{\partial u}{\partial n} - \rho\overline{u'v'} \tag{26}$$

188

and where s and n are orthogonal curvilinear coordinates in the plane of the flow oriented in the streamwise and cross-stream directions, respectively. Equation (23) thus represents the cumulative effect of such cross-stream stress gradients in the downstream direction.

The use of equation (23) to model the actual stagnation pressure distribution along $\psi = \psi_s$ in a separation bubble involves the assumption that the modification of the shear stress distribution due to the abrupt rise in static pressure at the rear of the bubble is small, or, equivalently, that the turbulent shear stresses are dominated by "memory" effects. Such an approximation of memory-dominated shear stresses is familiar in many analyses of turbulent flows following entry into a region of severe adverse pressure gradient (see especially refs. 20 and 18). The validity of this approximation when applied to the bubble problem has yet to be established, however.

With due regard for this uncertainty, we may take the nondimensional form of equation (24) as our working equation for the distribution of stagnation pressure along the streamline $\psi = \psi_s$:

$$\frac{H}{\frac{\rho}{2} U_s^2} = \frac{p}{\frac{\rho}{2} U_s^2} + \left(\frac{u}{U_s}\right)^2 \approx \frac{p_s}{\frac{\rho}{2} U_s^2} + \left(\frac{u}{U_s}\right)^2_{\substack{\text{plane} \\ \text{layer}}} \tag{27}$$

where the last term on the right-hand side is given by equation (23).

GASTER'S BURSTING CRITERION

M. Gaster (ref. 14) has obtained an empirical correlation in terms of the parameters R_{θ_s} and the pressure gradient parameter $\bar{P}$, defined by

$$\bar{P} = \frac{U_r - U_s}{x_r - x_s} \frac{\theta_s^2}{\nu} = \frac{(U_r - U_s)/U_s}{(x_r - x_s)/\theta_s} \frac{U_s \theta_s}{\nu} \tag{28}$$

that distinguishes between flow conditions permitting a short separation bubble and the conditions when a short bubble is not possible (i.e., a "bursting" condition). Figure 8 shows Gaster's so-called "bursting line," which we will attempt to derive from equation (27).

If we define a pressure coefficient c_p^* relative to the free stream conditions at the separation point in a bubble, then

$$\frac{p - p_s}{\frac{\rho}{2} U_s^2} = c_p^* = 1 - \left(\frac{u}{U_s}\right)^2 = \frac{c_p - c_{p_s}}{1 - c_{p_s}} \tag{29}$$

where $c_p = 1 - (U/U_\infty)^2$ is the conventional pressure coefficient. In terms of c_p^*, equation (27) becomes, on $\psi = \psi_s$,

$$c_p^* + \left(\frac{u}{U_s}\right)^2 = \left(\frac{u}{U_s}\right)^2_{\substack{\text{plane} \\ \text{layer}}} \tag{30}$$

At the reattachment point, the streamwise velocity u on $\psi = \psi_s$ equals zero, so that

$$\begin{pmatrix}\text{Reattachment} \\ \text{condition}\end{pmatrix} \qquad \sigma = c_{p_r}^* = \left(\frac{u}{U_s}\right)^2_{\substack{\text{plane} \\ \text{layer}}} \tag{31}$$

where the pressure recovery coefficient σ is the same as in equation (1).

Equation (31) together with equation (28), which at reattachment can be written as

$$\bar{P} = \frac{\sqrt{1 - c_{pr}^*} - 1}{(x - x_s)/\theta_s} R_{\theta_s} \tag{32}$$

define the largest possible $\bar{P}$ that can be achieved by a short bubble at a given R_{θ_s}. That is, if c_{pr}^* from equation (31) is substituted into equation (32) and the resulting $\bar{P}$ tabulated as a function of $(x - x_s)/\theta_s$ for a particular R_{θ_s}, then an extremum of $\bar{P}$ is found. For the Reynolds numbers $R_{\theta_s} = 100, 200, 300,$ and 400, we find that the extreme values of $\bar{P}$ are $-0.0996, -0.1868, -0.2732,$ and -0.3593, occurring at $(x - x_s)/\theta_s = 103, 111, 115,$ and 117, respectively. A faired curve through these points is shown in figure 8 and exhibits suprisingly good qualitative agreement with Gaster's empirical curve.

The agreement between theory and experiment is particularly pleasing in view of the fact that all of the empirical input to the present calculation method was obtained from measurements of transition in free shear layers in zero pressure gradient at a remote distance from any wall. Our calculations therefore lend support to the view that the processes of bubble bursting and shear layer reattachment are linked to the processes of laminar-turbulent transition and shear layer growth in a fundamental way.

COMPARISON WITH EXPERIMENTAL BUBBLE LENGTHS

As a caution against overly optimistic conclusions drawn from the present analysis, we present in figure 9 the results of an attempt to verify the reattachment condition (31) directly. In the figure, we have plotted the measured pressure recovery coefficient σ and length $(x_r - x_s)/\theta_s$ for a number of separation bubbles from various sources. On the same scale, we have drawn a copy of figure 7, which represents the nondimensional stagnation pressure along the separation streamline for a plane layer. If equation (31) held exactly, then all of the experimental points would lie on the dashed curves.

In fact, the experimental points are scattered quite widely about the analytic curves. More serious than the scatter in σ, however, is the discrepancy between the measured length of the bubbles, which are typically in the range $150 \lesssim (x_r - x_s)/\theta_s \lesssim 300$, and the values calculated from our analytic derivation of Gaster's bursting line. We have indicated the latter points in figure 9 by "plus" symbols, which lie, to within graphical accuracy, on the family of straight lines drawn through the origin and the points of tangency

with the various curves of $(u/U)^2_{\psi=\psi_s}$ for the plane layer. As can be seen,

the calculated bubble lengths are typically a factor two or three too small. This error is significant, and indicates that the present theory is not sufficiently refined for practical use in the quantitative prediction of bubble lengths.

It is not clear which of the many effects neglected in the theory are responsible for this discrepancy. We may speculate, however, that the neglect of changes in the shear stress gradient $\partial\tau/\partial n$ on the separation streamline during reattachment is important. Some such change must occur, since in the real flow the shear stress on $\psi = \psi_s$ vanishes at reattachment, which places the reattachment point below the point of maximum τ in the layer. The crude theory developed above assumes that as the separation streamline gets swallowed up into the underside of the shear layer, the shear stresses on the streamline tend asymptotically toward the value of the center of the layer (which is the maximum value). It follows that $\partial\tau/\partial n$ is underestimated by the crude theory. This implies (from equation (25)) an unrealistically low prediction of the stagnation pressure H. It is not obvious how the present theory could be refined to take such effects into account.

CONCLUSIONS

From our investigation of the physics of separation bubbles, we may state the following tentative conclusions:

1. The form of the static pressure distribution about a short separation bubble can be explained qualitatively in terms of boundary layer concepts. In particular, the sharp corner in the pressure distribution at the rear of a short bubble is more properly interpreted as the point where the lower edge of the reattaching shear layer grazes the surface than as the point of transition from laminar to turbulent flow, as has traditionally been assumed.

2. The observation that the static pressure distribution about the body on which a short separation bubble occurs very nearly coincides with the inviscid pressure distribution at all points other than those between separation and reattachment leads to a plausible hypothesis regarding the factors controlling bubble bursting and a simple but crude calculation method for estimating the length of a short bubble when it is possible for one to exist. Specifically, the reattachment point x_r coincides with the earliest downstream station x at which the stagnation pressure on the separation streamline is large enough to support an abrupt rise to the local inviscid static pressure at x.

3. The attempt to approximate the rise in stagnation pressure on the separation streamline in a bubble by the corresponding rise along a streamline entrained into the underside of a laminar mixing layer undergoing transition leads to a reasonably accurate prediction of Gaster's bursting line, but significantly underestimates the length of short bubbles in general. This inaccuracy is probably due to the failure of the calculation method to take account of changes in the viscous and turbulent shear stress profiles occurring prior to reattachment that produce (according to equation (25)) an increase in the actual stagnation pressure along the separation streamline beyond what exists in a free shear layer.

4. The present results are in every way consistent with and support the view of Cebeci and Bradshaw and others that reattachment is a direct consequence of the increased entrainment of fluid into the underside of the growing separated shear layer downstream of transition, the entrainment causing the shear layer to suck itself back down onto the surface.

APPENDIX

We rewrite equation (15) in the equivalent form

$$\int_0^\infty \left[(1 - f') - (1 - f')^2 \right] d\eta = \int_{-\infty}^0 (f')^2 \, d\eta \tag{A1}$$

Substituting equations (12) and (13) into equation (A1) gives

$$\left\{ \left[1 - f'(0) \right] I_1 - \left[1 - f'(0) \right]^2 I_2 \right\} \frac{1}{a} = I_3 \frac{f'(0)^2}{b} \tag{A2}$$

where

$$I_1 = \int_0^\infty \left(\frac{2}{\sqrt{\pi}} \int_{a\eta/2}^\infty e^{-x^2} \, dx \right) a \, d\eta = \frac{2}{\sqrt{\pi}} \tag{A3}$$

$$I_2 = \int_0^\infty \left(\frac{2}{\sqrt{\pi}} \int_{a\eta/2}^\infty e^{-x^2} \, dx \right)^2 a \, d\eta = \frac{2}{\sqrt{\pi}} \left(2 - \sqrt{2} \right) \tag{A4}$$

and

$$I_3 = \int_{-\infty}^0 \left\{ \frac{3}{2} \operatorname{sech}^2 \left[b\eta + \tanh^{-1} \left(\frac{1}{\sqrt{3}} \right) \right] \right\}^2 b \, d\eta = \frac{4\sqrt{3} - 9}{6} \tag{A5}$$

(assume $b < 0$ throughout)

The right-hand side of equation (A2) can be rewritten by means of equation (14) as

$$\frac{I_3 \, f'(0)^2}{b} = I_3 \frac{-f'(0)^3}{1 - f'(0)} \frac{2\sqrt{\pi}}{\sqrt{3}} \frac{1}{a} \tag{A6}$$

Substituting the identity

$$-f'(0)^3 = \left[1 - f'(0) \right]^3 - 3 \left[1 - f'(0) \right]^2 + 3 \left[1 - f'(0) \right] - 1$$

193

into equation (A6) and combining with equation (A2) gives the cubic equation

$$\left[1 - f'(0)\right]^3 \left(-I_2 - I_3 \frac{2\sqrt{\pi}}{\sqrt{3}}\right) + \left[1 - f'(0)\right]^2 \left(I_1 + 3I_3 \frac{2\sqrt{\pi}}{\sqrt{3}}\right)$$

$$+ \left[1 - f'(0)\right]\left(-3I_3 \frac{2\sqrt{\pi}}{\sqrt{3}}\right) + I_3 \frac{2\sqrt{\pi}}{\sqrt{3}} = 0 \qquad (A7)$$

which may be solved numerically by Newton's method to give the solution $1 - f'(0) = 0.41077$, or $f'(0) = 0.58923$.

The constants a and b may be calculated from the normalization condition (16) in the following way. The first integral on the right-hand side of equation (16) may be written

$$\int_{-\infty}^0 \left[f' - (f')^2\right] d\eta = \frac{f'(0)}{b} I_4 - \frac{f'(0)^2}{b} I_3$$

$$= \left[\frac{-f'(0)}{1 - f'(0)} \frac{2\sqrt{\pi}}{\sqrt{3}}\right] \frac{1}{a}\left\{f'(0) I_4 - \left[f'(0)\right]^2 I_3\right\} \qquad (A8)$$

where we have used equation (14), and where

$$I_4 = \int_{-\infty}^0 \frac{3}{2} \operatorname{sech}^2\left[b\eta + \tanh^{-1}\left(\frac{1}{\sqrt{3}}\right)\right] b \, d\eta = \frac{\sqrt{3} - 3}{2} \qquad (A9)$$

The second integral on the right-hand side of equation (16) is just the left-hand side of equation (A2). According to equation (16), the sum of these two integrals equals $-f(-\infty) = 1.2386$, which immediately gives $a = 0.88544$. Equation (14) then gives $b = -0.30160$.

REFERENCES

1. Jones, B. Melvill: An Experimental Study of the Stalling of Wings.
   R. & M. No. 1588, British A.R.C., 1934.

2. Tani, Itiro: Low Speed Flows Involving Bubble Separations. Progress in
   the Aeronautical Sciences, D. Kuechemann, ed., vol. 5, 1964.

3. Schmitz, F. W.: Zur Aerodynamik der Kleinen Reynoldszahlen. Jb. 1953
   Wiss. Ges. Luftfahrt. Brauschweig 1954, S. 149/166.

4. Kraemer, K.: Fluegelprofile im Kritischen Reynolds-zahl-Bereich. Forschung
   auf dem Gebiete des Ingenieurwesens, Band 27, S. 33/46.

5. Young, A. D.: Some Special Boundary Layer Problems. 20th Ludwig Prandtl
   Lecture. Zeit. Flugwiss. u. Weltraumforschung, Band 1, S. 401/414, 1977.

6. Crimi, P.; and Reeves, B. L.: Analysis of Leading Edge Separation Bubbles
   on Airfoils. AIAA J., vol. 14, pp. 1548-1554, 1976.

7. Briley, W. R.; and McDonald, H.: Numerical Prediction of Incompressible
   Separation Bubbles. J. Fluid Mech., vol. 69, pp. 631-656, 1976.

8. Geropp, D.; und Grashof, J.: Berechnumg von Stroemungsfeldern mit
   Abloeseblasen bei Grossen Reynoldszahlen. DLR-FB 76-52, Institut fuer
   Stroemungslehre und Stroemungsmachinen, Universitaet Karlsruhe, 1976.

9. Cebeci, T.; and Bradshaw, P.: Momentum Transfer in Boundary Layers. New
   York: McGraw-Hill, 1977.

10. Gault, Donald E.: An Experimental Investigation of Regions of Separated
    Laminar Flow. NACA TN 3505, 1955.

11. Ingen, J. L. van: On the Calculation of Laminar Separation Bubbles in Two-
    Dimensional Incompressible Flow. In AGARD CP-168: "Flow Separation,"
    Goettingen, 1975.

12. Sato, Hiroshi: Experimental Investigation of the Transition of Laminar
    Separated Layer. J. Phys. Soc. Japan, vol. 11, pp. 702-709, 1956.

13. Owen, P. R.; and Klanfer, L.: On the Laminar Boundary-Layer Separation
    From the Leading Edge of a Thin Aerofoil. British A.R.C. C.P. 220, 1953.

14. Gaster, M.: The Structure and Behavior of Laminar Separation Bubbles.
    British A.R.C. R. & M. 3575, 1969.

15. Lock, R. C.: The Velocity Distribution in the Laminar Boundary Layer
    Between Parallel Streams. Quart. J. Mech. and Appl. Math., vol. 4,
    pp. 42-63, 1951.

16. Liepmann, H. W.; and Laufer, J.: Investigations of Free Turbulent Mixing.
    NACA TN 1257, 1947.

17. Schlichting, H.: Boundary Layer Theory, 6th edition, J. Kestin, trans.,
    New York: McGraw-Hill, 1968.

18. Townsend, A. A.: The Structure of Turbulent Shear Flow. Cambridge:
    Cambridge University Press, 1976.

19. Freymuth, Peter: On Transition in a Separated Laminar Boundary Layer.
    J. Fluid Mech., vol. 25, pp. 683-704, 1966.

20. Stratford, B. S.: The Prediction of Separation of the Turbulent Boundary
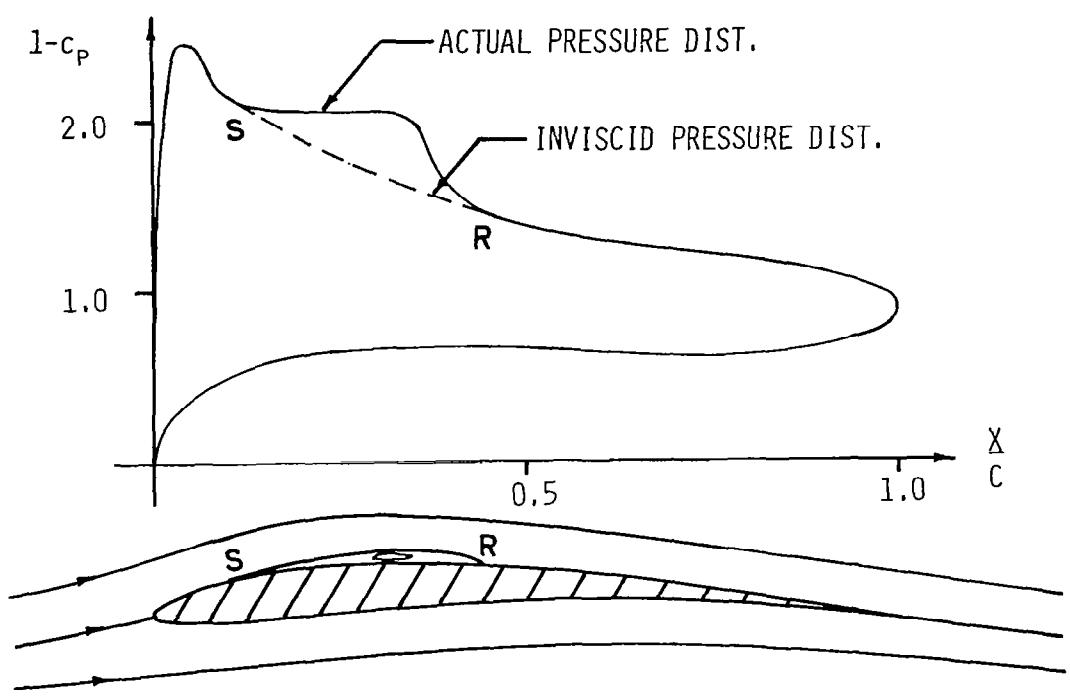   Layer. J. Fluid Mech., vol. 5, pp. 1-16, 1959.

Figure 1.- Characteristic pressure distribution beneath a
separation bubble of the "short" type.
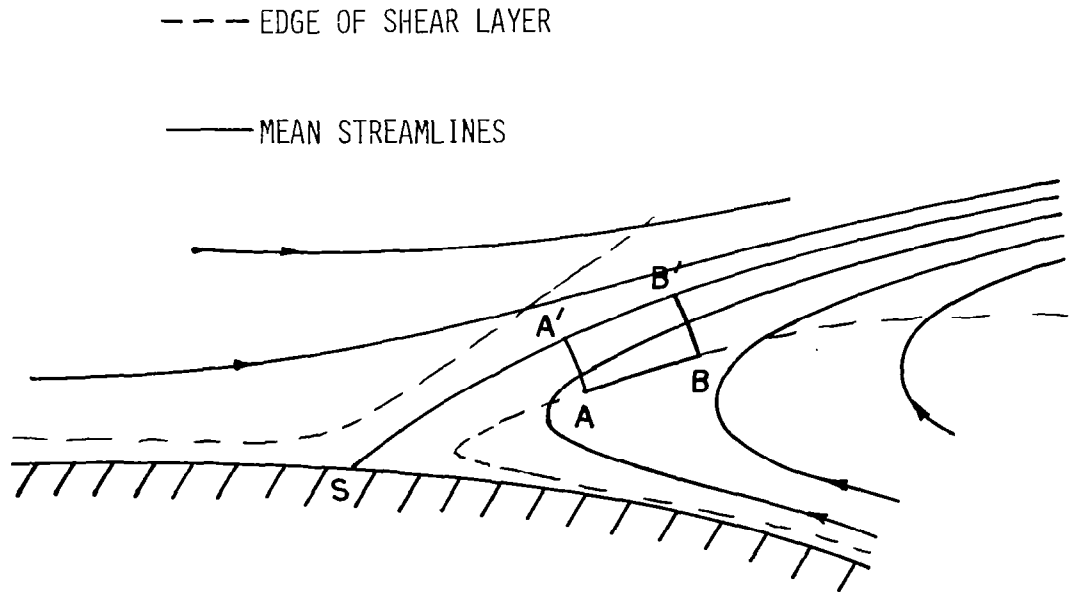
Figure 2.- Two-dimensional steady separation from a
solid wall showing entrainment of fluid into the
underside of the shear layer due to spreading in
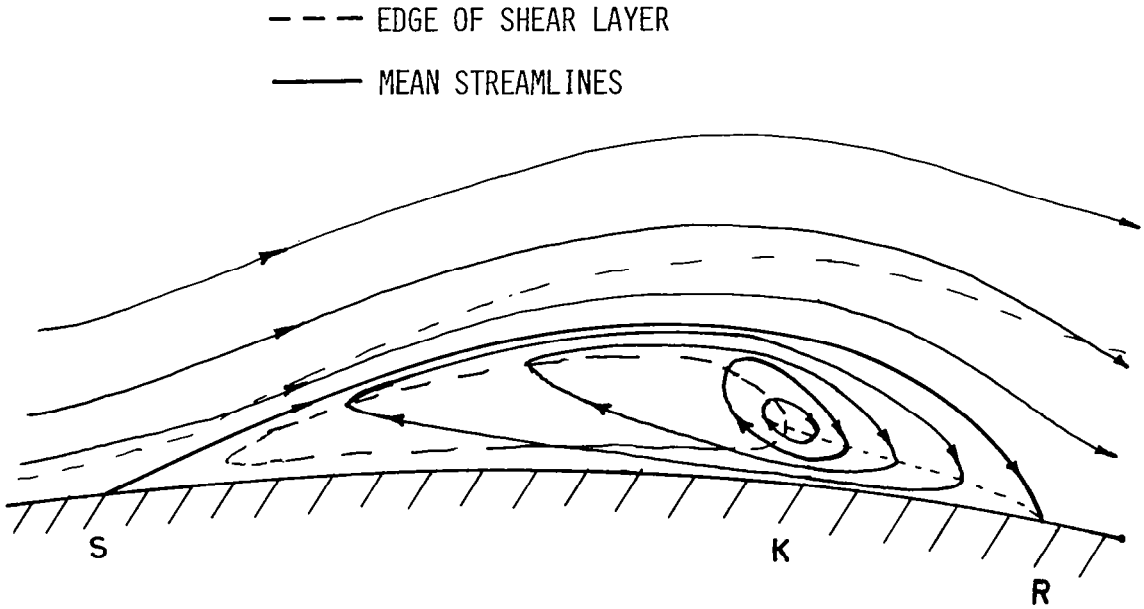the downstream direction.

Figure 3.- Recirculating flow pattern within a bubble
showing splitting of the shear layer at reattach-
ment to supply the entrainment (vertical scale
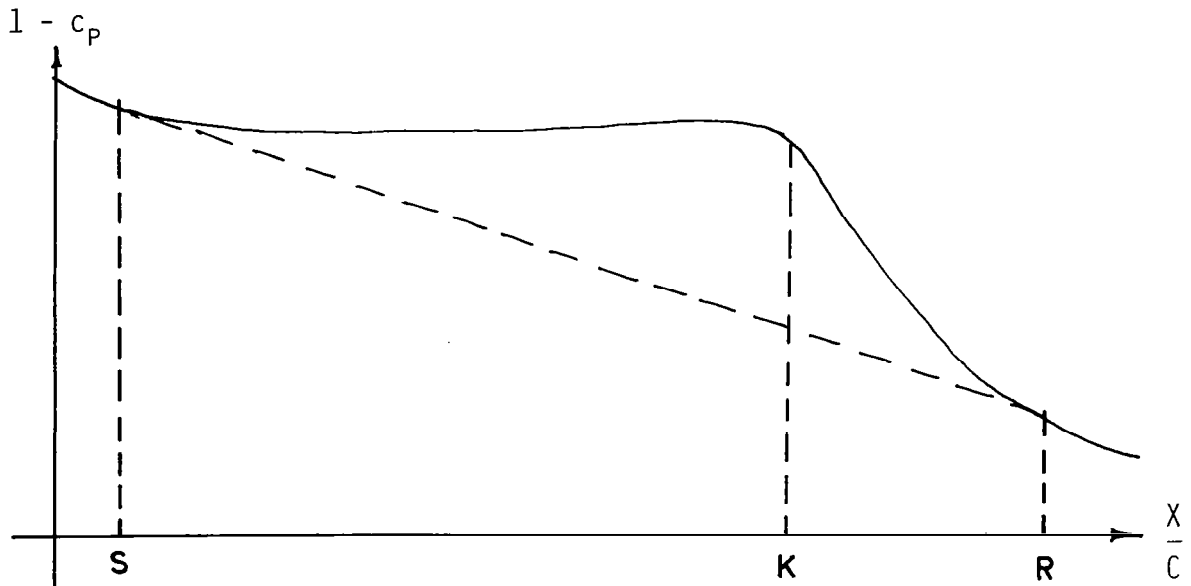greatly exaggerated).

Figure 4.- Pressure distribution inferred from figure 3.
Small entrainment velocities beneath shear layer imply
small pressure gradients between S and K. Steep
gradient between K and R due to splitting of shear
layer at reattachment and gradient of stagnation pres-
sure across lower half of shear layer.
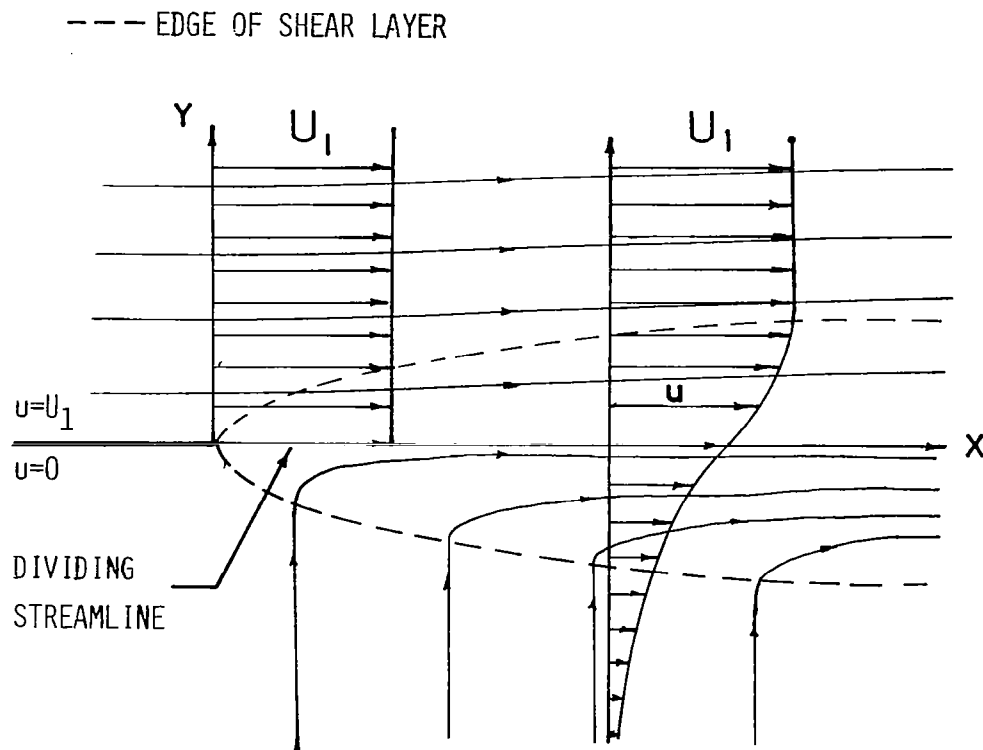
--- EDGE OF SHEAR LAYER

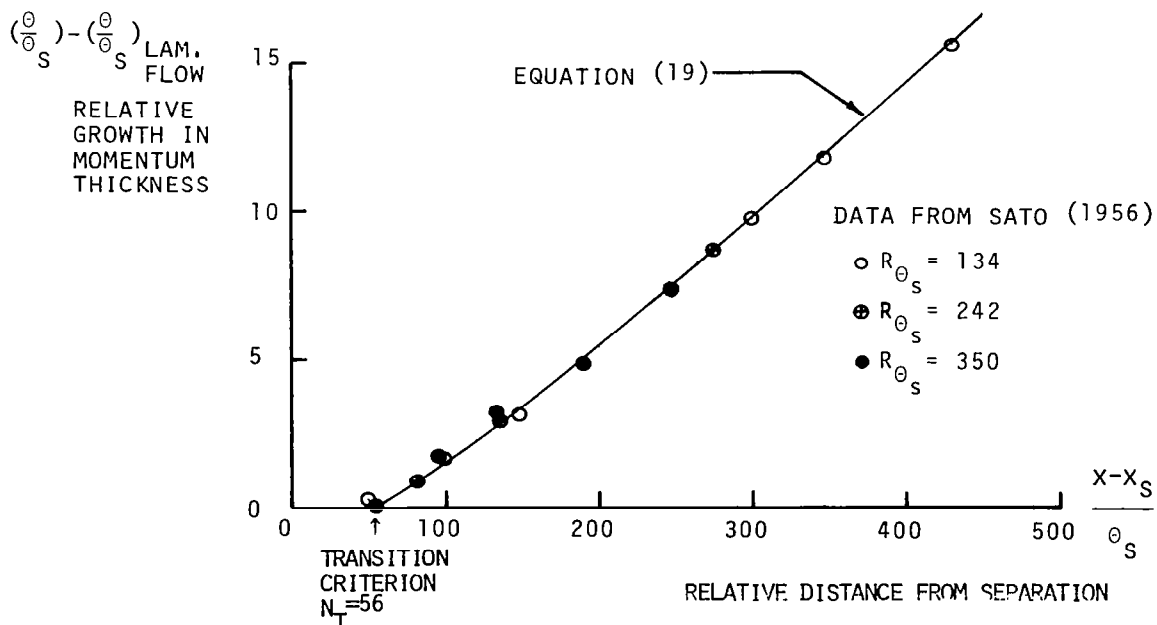Figure 5.- Nomenclature for free shear layers in
zero pressure gradient.

Figure 6.- Verification of empirical formula for growth of momentum
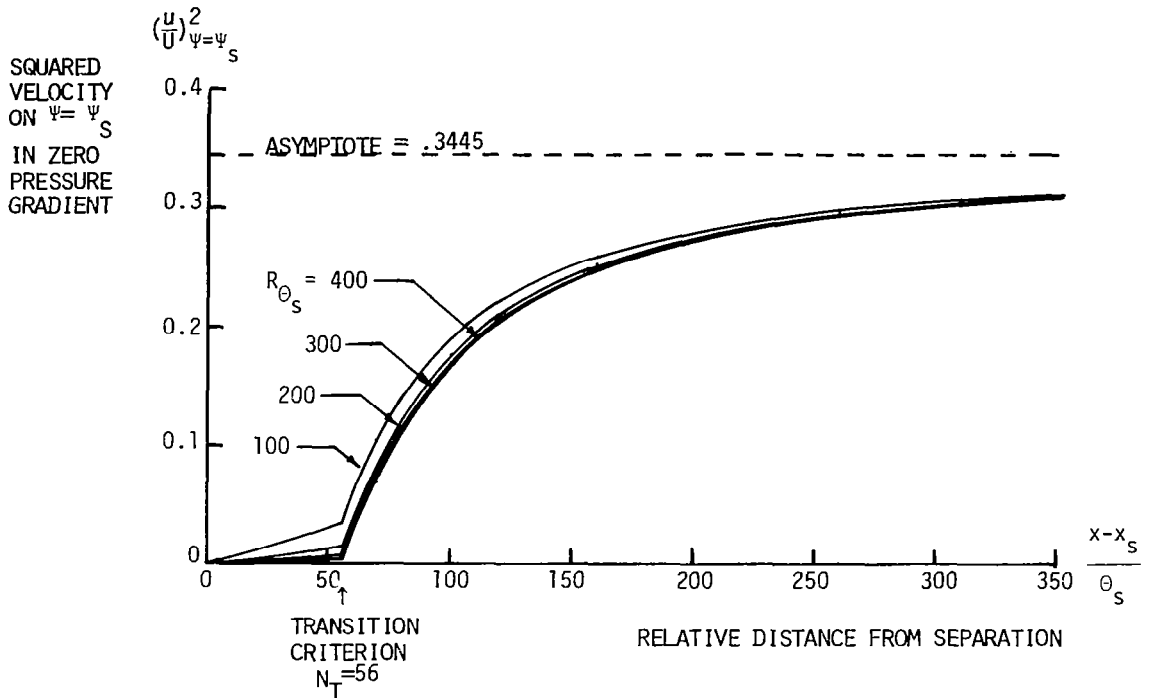thickness downstream of transition. Data from reference 12.

$$\left(\frac{u}{U}\right)^2_{\Psi=\Psi_s}$$

SQUARED
VELOCITY
ON $\Psi = \Psi_s$
IN ZERO
PRESSURE
GRADIENT

0.4

ASYMPTOTE = .3445

0.3

$R_{\Theta_s} = 400$

300

200

0.2

100

0.1

0

0   50   100   150   200   250   300   350 $\dfrac{x-x_s}{\Theta_s}$

TRANSITION
CRITERION
$N_T = 56$

RELATIVE DISTANCE FROM SEPARATION

Figure 7.- Plot of equation (23) using equations (17), (18), and (19).

$$\bar{P} = \frac{\Delta u}{\Delta x}\frac{\Theta_s^2}{\nu}$$

STRENGTH OF
ADVERSE
PRESSURE
GRADIENT

-0.4

GASTER'S BURSTING
LINE (1956)

-0.3

(SHORT BUBBLES IMPOSSIBLE)

-0.2

PRESENT THEORY

(SHORT BUBBLES POSSIBLE)

-0.1

($\bar{P} \geq -.09$ IMPLIES
FULLY ATTACHED LAMINAR FLOW)

0

0   100   200   300   400 R_{Θ_s}
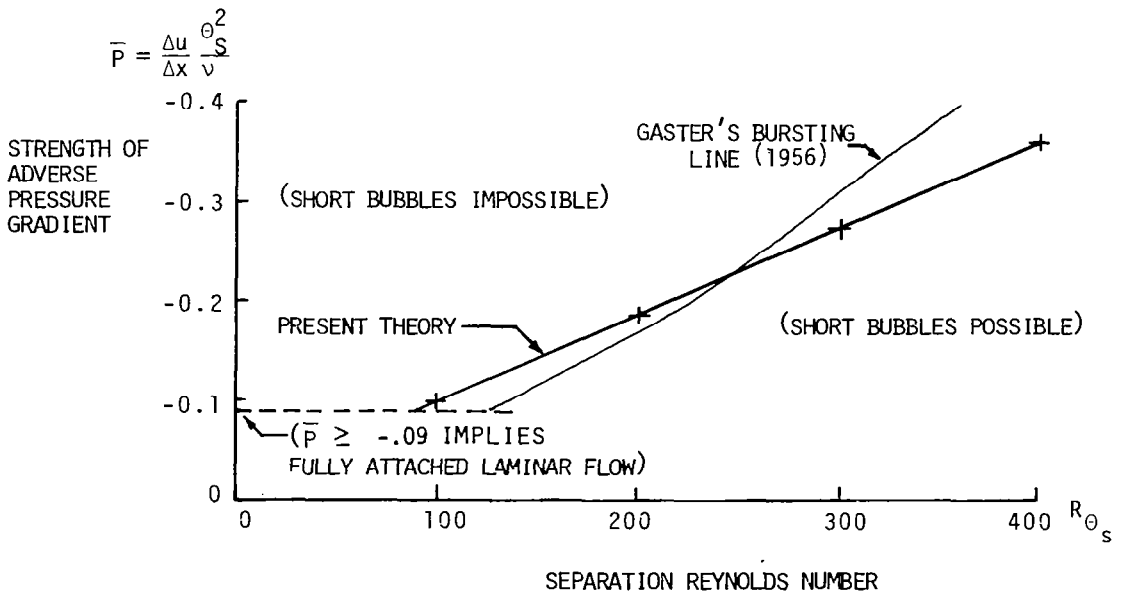
SEPARATION REYNOLDS NUMBER

Figure 8.- Gaster's bursting line derived from present theory,
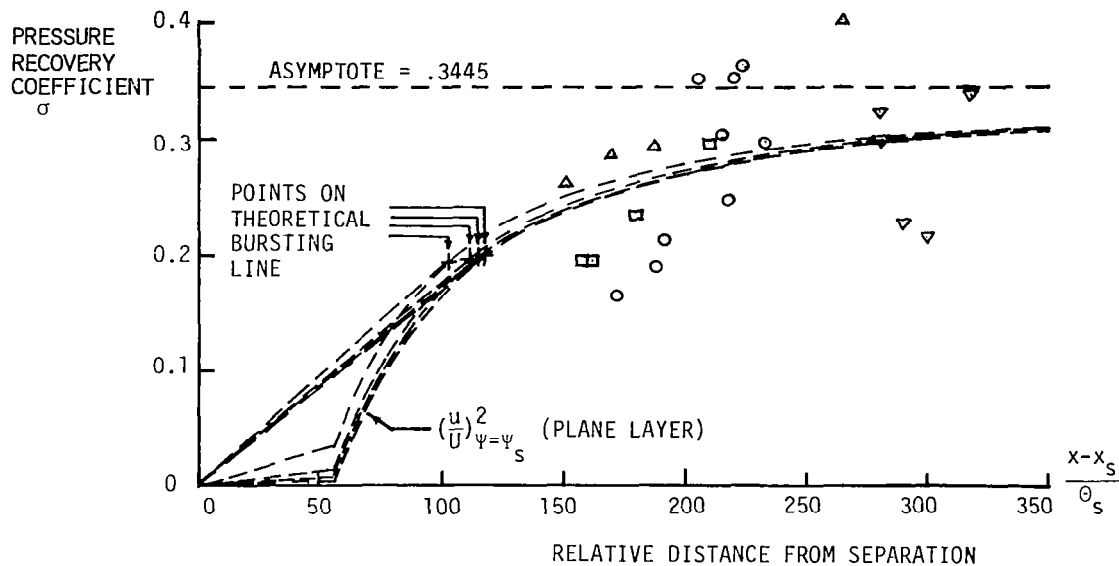which is based entirely on data from free shear layers.

Figure 9.- Attempt to verify reattachment condition (31).
Measured lengths and pressure recovery coefficients
from various sources: □, Gaster (ref. 14) "series I";
△, Gaster "series II"; ○, Van Ingen (ref. 11); ▽, Tani
(ref. 2, fig. 17, based on data from Gault, ref. 10).
If equation (31) held exactly, then all measured points
should lie on dashed curves. Note: each set of data
represents a series of runs at various tunnel speeds,
which, to avoid cluttering the figure, have not been
shown.